Physics of Plasmas

RESEARCH ARTICLE | DECEMBER 11 2023

Stationary Bragg reflection of laser light in inhomogeneous absorbing plasmas inside inertial confinement fusion *Hohlraums* FREE

M. Vandenboomgaerde ; M. Casanova; F. Chaland ; M. Bonnefille ; A. Grisollet ; L. Videau ; S. Depierreux ; V. Tassin ; J.-P. Leidinger; C. Courtois ; J. Garnier ; H. Chen

Phys. Plasmas 30, 122702 (2023)
https://doi.org/10.1063/5.0170189

Physics of Plasmas ARTICLE pubs.aip.org/aip/pop

Stationary Bragg reflection of laser light in inhomogeneous absorbing plasmas inside inertial confinement fusion *Hohlraums*

Cite as: Phys. Plasmas **30**, 122702 (2023); doi: 10.1063/5.0170189
Submitted: 1 August 2023 · Accepted: 19 November 2023 ·
Published Online: 11 December 2023

M. Vandenboomgaerde,[1,a)] M. Casanova,[1] F. Chaland,[1] M. Bonnefille,[1] A. Grisollet,[1] L. Videau,[1] S. Depierreux,[1] V. Tassin,[1] J.-P. Leidinger,[1] C. Courtois,[1] J. Garnier,[2] and H. Chen[3]

AFFILIATIONS

[1]CEA, DAM, DIF, F-91297 Arpajon, France
[2]Centre de Mathématiques Appliquées, Ecole Polytechnique, Institut Polytechnique de Paris, F-91128 Palaiseau, France
[3]Lawrence Livermore National Laboratory, Livermore, California 94550, USA

[a)]Author to whom correspondence should be addressed: marc.vandenboomgaerde@cea.fr

ABSTRACT

Laser-produced plasma in inertial confinement fusion (ICF) *Hohlraums* are marked with density non-uniformity whose length scale can go down to micrometers. This scale is of the order of the laser wavelength. The WKB approximation, which is classically used in radiation-hydrodynamic codes to compute the laser trajectory, cannot correctly take into account such small-scale inhomogeneity of the plasma. Going beyond this approximation, we predict a novel mechanism for the laser reflection. We show that an electromagnetic plane wave with wave number k resonates with the $k_B = 2\,k$ Fourier component of a multimode perturbation of the background density and generates a reflected wave. It is the first time that this reflection is considered for stationary inhomogeneous ICF plasmas, and the energy absorption is taken into account. This mechanism, which is a form of Bragg reflection, can occur away from the critical surface and generate a drift of the location of the laser absorption. Furthermore, this absorption will be periodically modulated with a k_B wave number. The stationary Bragg reflection can explain ongoing discrepancies between experimental and numerical data about laser trajectory and absorption in ICF *Hohlraums*.

I. INTRODUCTION

In indirect-drive inertial confinement fusion (ICF) experiments, the x-ray drive around the fuel pellet must be highly symmetric. This drive is generated by the conversion of the laser absorption at the *Hohlraum* wall. As a result, the control and optimization of the laser deposition is crucial for the success of ICF. For years, discrepancies between experimental data and numerical simulations have pointed out that the laser deposition is not accurately predicted by radiation-hydrodynamic (rad-hydro) codes.[1–9] Some of the proposed mechanisms to explain such discrepancies are regional heat conduction flux,[8,10] cross beam energy transfer (CBET),[6,11–14] and stimulated scattering processes, Brillouin (SBS), and Raman (SRS).[11,15,16]

In ICF *Hohlraums*, the dynamics of the plasma is quite complex: spatially evolving hydrodynamic phenomena such as shock waves, ablation fronts, plasma collisions, hydrodynamic instabilities[17,18] at interfaces or turbulence[19–21] superimpose with self-generated magnetic fields, microinstabilites, and abrupt temporal changes of the internal and radiation energies. This complexity generates a multi-scale inhomogeneity of the plasma density and, thus, of the electronic density. Micron-scale phenomena have been recently observed in high energy density experiments.[21] Most of the rad-hydro codes rely on ray-tracing packages to compute the laser trajectory and absorption. These packages use the WKB approximation. As a result, the effect on the laser trajectory of plasma index inhomogeneity, which length scale is of the order of the laser wavelength, cannot be correctly taken into account. In ICF standard computations, this issue is usually not considered as rad-hydro codes can only track mean flow variations with a typical length scale of few tens of micrometers.

In this paper, we propose and study a novel mechanism that could affect laser trajectory and absorption in ICF plasmas and explain recent experimental observations. Some multimode spatial variations of the background electronic density (starting from sub-micron length scale) are assumed. Their lifetimes are supposed far greater than the time needed by the laser to pass through as well as spatial extensions greater than several laser wavelengths. Going beyond the WKB approximation, we theoretically and numerically demonstrate in the

one-dimensional (1D) geometry that a plane electromagnetic (em) wave with wave number k self-selects and resonates with the $k_B = 2\,k$ Fourier component of the electronic density profile. Wave reflection can then occur far from the critical surface in a plasma where small-scale inhomogeneity exists. In such a plasma, computations show that the maximum of laser absorption moves away from the critical density. Furthermore, the influence of the energy absorption on the wave trajectory differs from the WKB modeling. These results could help understanding discrepancies between experiments and numerical simulations about the implosion symmetry of ICF capsule, or the x-ray emission maps of the laser-heated *Hohlraum* wall.[1,7,8]

The paper is organized as follows. Section II summarizes the standard derivation for wave trajectory and absorption in the WKB approximation. Then, when no approximation is done, the resonance of an em wave with the $2\,k$ mode of the electronic density profile is demonstrated as well as the generation of a reflected wave. In Sec. III, the reflectivity of a plasma due to a small-scale inhomogeneity is estimated. In Sec. IV, the full-wave solution of the wave equation is computed for several profiles of the electronic density inhomogeneity in order to support the theoretical results about the resonance and its k_B mode selection. In Sec. V, the relation with the classical Bragg reflection in Tokamak plasma, and specificities of this reflection are discussed. Then, in Sec. VI, distinction between this mechanism and classical parametric instabilities is underlined. Section VII assesses the existence of small-scale plasma inhomogeneity in the gold bubble of ICF *Hohlraums*. In Sec. VIII, effects on the laser absorption and plasma properties are considered. They are applied to the analysis of an experiment. Section IX concludes this paper.

II. THEORETICAL MODELING OF LASER TRAJECTORY AND ABSORPTION

For a 1 cm ICF under-dense plasma, the timescale of the laser travel is $\tau_T \approx 3.3\,10^{-11}$ s. Let us define the hydrodynamic timescale, τ_H, as the time needed for the gold bubble plasma of an ICF *Hohlraum* to travel 1 cm. Numerical simulations give a value for τ_H about several nanoseconds. In the following, as $\tau_T \ll \tau_H$, the plasma is considered as almost frozen on the timescale of the laser wave, i.e., ion motion is neglected. The plasma is also assumed neutral, and the electronic density inhomogeneity follows the density variation. For simplicity, this stationary plasma is taken one-dimensional (1D) with the electronic density varying in the x-direction (Fig. 1). Consider a plane em wave propagating into this static plasma. The E field of the wave is written as

$$E(x,t) = E_0 e^{i(\omega_0 t - \phi(x))}\,, \tag{1}$$

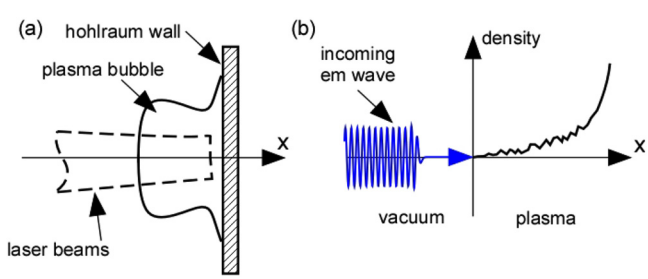

FIG. 1. (a) Schematic of a laser heated *Hohlraum* wall. (b) 1D studied configuration.

where ω_0 is the laser frequency, and $k(x) = k_r(x) + i\,k_i(x) = \partial\phi(x)/\partial x$ is the laser wave number. Combining the Maxwell's equations and the momentum equation for the electrons, the coupling between the light wave and the electron plasma can be described. The subsequent wave equation[22–24] is written as follows [for sake of simplicity, the (x, t) dependency of E, and the x dependency of other variables will be dropped in the following equations]:

$$\frac{\partial^2 E}{\partial x^2} - \frac{1}{c^2}\frac{\partial^2 E}{\partial t^2} - \frac{\omega_p^2}{c^2}\frac{E}{1 - i\,\dfrac{\nu_{ei}}{\omega_0}} = 0\,, \tag{2}$$

where c is the light velocity in vacuum, ω_p is the plasma frequency, and ν_{ei} is the electron ion collision frequency. Exact analytical solutions of the wave equation are known only for a few plasma permittivity profiles. For other profiles, if the permittivity variation takes place on a length scale much larger than the local laser wave wavelength, $\lambda(x)$, i.e., the permittivity is a slowly varying function, the reflection is weak and the first geometrical optics approximation[22,25] can be used to solve Eq. (2). This approximation is equivalent to the WKB approximation. The latter implies that, whatever the function $f(x)$ describing a physical property, $\partial f(x)/\partial x\,\lambda(x) \ll f(x)$. If the permittivity profile varies on shorter length scale, a useful strategy has been to discretize the plasma as a large number of thin homogeneous layers. In each layer, the E field is written as the sum of an incoming and a reflected plane em waves, $E(x,t) = E_i\,e^{i(\omega_0 t - kx)} + E_r\,e^{i(\omega_0 t + kx)}$. The transfer matrix method[25,49,50] and proper boundary conditions at the interfaces can be used to determine the discretized E field.

In the following, we solve Eq. (2) for a slowly varying background density profile and a superimposed arbitrary multi-scale inhomogeneity. The form of the solution is kept as Eq. (1), and a perturbation method determines the function $k(x)$ beyond the WKB approximation. Then, a Jacobi–Anger expansion of the resulting E field shows how the reflected wave builds from the interaction between the incoming wave and the plasma inhomogeneity.

Introducing Eq. (1) into Eq. (2), the real and imaginary parts read

$$\begin{cases} \dfrac{\partial k_i}{\partial x} - k_r^2 + k_i^2 + \dfrac{\omega_0^2}{c^2}\left(1 - \dfrac{\omega_p^2}{\omega_0^2}\dfrac{1}{1 + \left(\dfrac{\nu_{ei}}{\omega_0}\right)^2}\right) = 0, \\[2ex] \dfrac{\partial k_r}{\partial x} + 2k_r k_i + \dfrac{\omega_p^2}{c^2}\dfrac{\dfrac{\nu_{ei}}{\omega_0}}{1 + \left(\dfrac{\nu_{ei}}{\omega_0}\right)^2} = 0. \end{cases} \tag{3}$$

Using the WKB approximation on $k(x)$ leads to $\partial k(x)/\partial x \ll k(x)^2$. In the framework of this approximation, Eqs. (3) are simplified, and can be solved analytically. Furthermore, if $\nu_{ei}/\omega_0 \ll 1$ is assumed, the following well-known expression[22,51,52] for $k(x)$ is derived:

$$\begin{cases} k_r = k_0\,n_r = k_0\sqrt{1 - \dfrac{n_e}{n_c}}, \\[2ex] k_i = k_0\,n_i = -\dfrac{k_0}{2}\dfrac{\nu_{ei}}{\omega_0}\dfrac{n_e/n_c}{\sqrt{1 - \dfrac{n_e}{n_c}}}, \end{cases} \tag{4}$$

where $k_0 = 2\pi/\lambda_0$, $n = n_r + i\,n_i$, n_e, and n_c are the laser wave number in vacuum, the complex index of the plasma, the electronic density, and the critical electronic density, respectively. The latter is defined by $\omega_0^2 = 4\pi\, n_c\, e^2/m_e$ with e and m_e, the electron charge and mass, respectively. The intensity, I, of the plane em wave is proportional to $n_r|E|^2$. If $n_r(x)$ is a slow varying function, this leads to $I = I_0\, e^{\int 2\,k_i(x)\,dx}$. In the WKB approximation, $k_i < 0$ and I decreases along the ray path due to the energy lost by electron–ion collisions. Equations (4) show that the laser deposition dI/dx drastically increases as $n_e \to n_c$. Equations (4) also show that the local wavelength of the em wave, $\lambda(x) = 2\pi/k_r(x)$, increases as $1/\sqrt{1 - n_e(x)/n_c}$. It is usual to note that the WKB approximation is not valid in the vicinity to n_c. Let us emphasize that, even far from n_c, the WKB approximation also cannot correctly handle the propagation of a wave in a plasma where some length scales are of the order of λ.

The response of an em wave to λ-scale electronic density ripples is now studied. The electronic density profile is written as $n_e(x) = \overline{n_e}(x) + \widetilde{n_e}(x)$, where $\overline{n_e}(x)$ is a slow varying function, $\widetilde{n_e}(x) = \sum_{p=1}^{\infty} N_p\, \cos\left(p \int_0^x \overline{k_r}(x)\,dx\right)$, with $N_p/\overline{n_e}(x) \ll 1$. The perturbation solution reads as $k = \overline{k} + \widetilde{k}$, with $\overline{k} = \overline{k_r} + i\overline{k_i}$ the WKB solution, and $\widetilde{k} = \widetilde{k_r} + i\widetilde{k_i}$ a first order correction ($\widetilde{k_r} \ll \overline{k_r}$, $\widetilde{k_i} \ll \overline{k_i}$). The first order expansion of Eqs. (3) gives, for $\nu_{ei}/\omega_0 \ll 1$, and slowly varying $\overline{k_r}$:

$$\begin{cases} \dfrac{\partial \widetilde{k_i}}{\partial x} - 2\,\overline{k_r}\,\widetilde{k_r} + 2\,\overline{k_i}\,\widetilde{k_i} - \dfrac{\overline{\omega_p}^2}{c^2}\dfrac{\widetilde{n_e}}{\overline{n_e}} = 0, \\ \dfrac{\partial \widetilde{k_r}}{\partial x} + 2(\overline{k_r}\widetilde{k_i} + \overline{k_i}\widetilde{k_r}) = 0. \end{cases} \tag{5}$$

Seeking solutions as $\widetilde{k_r}(x) = K_r(x)\, e^{-2\int_0^x \overline{k_i}(x)dx}$ and $\widetilde{k_i}(x) = K_i(x)\, e^{-2\int_0^x \overline{k_i}(x)dx}$ with $\widetilde{k_r}(0) = 0$, the following result is found for $\widetilde{k_r}(x)$:

$$\widetilde{k_r}(x) = \frac{\overline{\omega_p}^2}{c^2}\left[-\frac{x}{2}\frac{N_2}{\overline{n_e}}\, \sin\left(2\int_0^x \overline{k_r}\,dx\right) + \sum_{p\neq 2}\frac{N_p}{\overline{n_e}}\frac{2}{(p^2-4)} \times \left(\frac{\cos\left(p\int_0^x \overline{k_r}\,dx\right)}{\overline{k_r}} - \frac{\cos\left(2\int_0^x \overline{k_r}\,dx\right)}{k_0} \right)\right]. \tag{6}$$

Equation (6) shows that the value $p = 2$ leads to a secular term. In comparison with this secular response, the amplitude of the other modes is negligible for $x > 1/\overline{k_r}(x)$. This means that a plane em wave going through a plasma essentially resonates with the $p = 2$ Fourier mode of the density inhomogeneity profile. In other words, the em wave self-selects the $k_B(x) = 2\pi/\lambda_B(x) = 2/x \int_0^x \overline{k_r}(x)\,dx$ mode of the electronic density profile and interacts with it. Let us note that for is a slowly varying $\overline{k_r}(x)$, $k_B(x) \approx 2\,\overline{k_r}(x)$. Thus, solution (6) can be approximated as

$$\widetilde{k_r}(x) \approx -\frac{\overline{\omega_p}^2}{c^2}\frac{x}{2}\frac{N_2}{\overline{n_e}}\, \sin(2\overline{k_r}\,x)\,. \tag{7}$$

This solution shows that, when subjected to n_e inhomogeneities, the em wave sees its wave number $k_r(x)$ displaying increasing oscillations with x. Numerical integration of Eqs. (3) shows that the amplitude of these oscillations can be such that $k_r(x)$ reaches 0, i.e., wave reflection, even if $n_e(x) \neq n_c$.

Equation (1) can be expanded as $E(x,t) = E_0\, e^{\int_0^x k_i(x)dx} \times e^{i(\omega_0\, t - \int_0^x (\overline{k_r}(x) + \widetilde{k_r}(x))dx)}$. Then, Eq. (7) leads to

$$E = E_0\, e^{k_i\, x}\, e^{i(\omega_0\, t - \overline{k_r}\, x)}\, e^{-i\, z\, \cos(2\overline{k_r}\, x)}\, e^{i\, w\, \sin(2\overline{k_r}\, x)} \tag{8}$$

with $z = \alpha\,\overline{k_r}\,x$, $w = \alpha/2$, and $\alpha = \frac{1}{4}\frac{\overline{\omega_p}^2}{\overline{k_r}^2 c^2}\frac{N_2}{n_e(x)}$. Using the Jacobi–Anger expansion, $e^{\pm i\,a\,\sin b} = \sum_{m=-\infty}^{+\infty} J_m(a) e^{\pm imb}$, Eq. (8) gives

$$E = E_0\, e^{k_i\, x}\{J_0(z)J_0(w)e^{i(\omega_0\, t - \overline{k_r}\, x)} + (J_0(z)J_1(w) + iJ_0(w)J_{-1}(z))e^{i(\omega_0\, t + \overline{k_r}\, x)} + o.t.\}, \tag{9}$$

where o.t. stands for the other terms of the expansion product and represents the generation of harmonics. Equation (9) displays a counter-propagating em plane wave which amplitude depends on $N_2/\overline{n_e}(x)$. Thus, the modulation of $k_r(x)$ described by Eq. (7) can be interpreted as the signature of the superposition of the incoming wave and a reflected one. Going beyond the WKB approximation, we have analytically demonstrated how a bulk reflection is generated within a plasma by the direct interaction between the incoming wave and a static small-scale multimode inhomogeneity.

Let us note that $\widetilde{k_i}$ also displays oscillations, and the energy deposition is consequently modulated (see Sec. V). This could lead to a positive feedback on the density inhomogeneity (see Sec. VIII).

III. BULK REFLECTANCE DUE TO INHOMOGENEITY IN A STATIC PLASMA

In this section, we demonstrate a direct analogy between a wave interacting with a multimode modulated stationary plasma and a wave interacting with a quarter-wave stratified medium. Indeed, as seen above, a plane em wave propagating through multimode electronic density inhomogeneities interacts mainly with the k_B mode as if the n_e profile was $n_e(x) = \overline{n_e}(x) + N_2\, \cos(k_B\, x)$. The influence of the other modes of the inhomogeneity is negligible. So, the reflectance of a randomly inhomogeneous plasma can be emulated by a layered medium with a sinusoidal index modulation. In such a medium, the maximum reflectance is obtained for the k_B index modulation.[25–30] If the plasma index is written as $n_r(x) = \overline{n_r}(x) + \widetilde{n_r}\, \cos(k_B x)$ where $\overline{n_r}$ is a slowly varying function, and if the absorption is neglected, the reflectance is written as[30]

$$R = \tanh^2\left(\widetilde{n_r}\,\frac{\pi L}{\lambda_0}\right), \tag{10}$$

where L is the length of the plasma. If $N_2/\overline{n_e} \ll 1$, and far from the critical surface, the reflectance as a function of the electronic density perturbation is approximated by

$$R = \tanh^2\left(\frac{1}{2}\frac{N_2}{\overline{n_e}}\frac{\overline{n_e}/n_c}{\sqrt{1 - \overline{n_e}/n_c}}\frac{\pi L}{\lambda_0}\right). \tag{11}$$

Equation (11) shows that the reflectance rapidly increases with the amplitude of the electronic modulation, N_2, and the length of the

plasma, L. For example, the reflectance of a 100 μm plasma pocket at $\overline{n_e}/n_c = 0.5$ with electronic density inhomogeneity such that $N_2/\overline{n_e} = 0.01$ is $R = 0.993$ for a laser beam at $\lambda_0 = 0.35\mu$m. This plasma pocket will almost totally reflect the laser beam, even if far from the critical surface. Equation (11) also shows that the reflectance directly depends on the product $N_2\,L$. The same reflectance value as in the previous example is obtained for a much higher, maybe unrealistic, value of the n_e inhomogeneity magnitude, $N_2 = 0.1$, and a shorter plasma length, $L = 10\ \mu$m.

In Sec. IV, some of the numerical simulations will use this property of the reflectance: in order to reduce the size of the computation domain, and make resulting graphics more readable, high values of the electronic density modulation will be considered. These simulations are equivalent to others with smaller values of N_2 but longer computation domains.

IV. FULL-WAVE COMPUTATIONS

In order to support the conclusions drawn from the first order perturbative result of Sec. II, the sensitivity of an incoming em plane wave to electronic density inhomogeneity is now studied with 1D full-wave computations. The full-wave solution of the wave equation (2) has been numerically computed. Following Ref. 31, the second order Eq. (2) is split in two first order differential equations. The resulting system is solved by a partially implicit numerical scheme. The domain of computation is taken large enough in comparison with the domain of interest in order to first stabilize the source wave propagation and second to prevent any spurious reflected wave at the boundaries. The spatial grid resolution, Δx is equal to $\lambda_0/10$. This numerical model has been validated on sharp index gradients with the Fresnel's solution and on smooth gradients with analytic solutions. In order to check the secular response of an incoming wave to k_B inhomogeneity of the electronic density, we consider a collisionless plasma described by the index $n_r^2 = 1 - 0.9\,(X^2 - 1)^2$ with $X = (x - 100)/140$ for $-40 \le x \le 100$, $n_r^2 = 1$ for $x < -40$, and $n_r^2 = 0.1$ for $x > 100$. A periodic source field ($E_0 = 0.5$, $\lambda_0 = 2$, $\omega_0 = \pi/2$) is located at the negative x boundary. Thus, the em wave is emitted in vacuum, encounters a density gradient, and reaches $n_e/n_c = 0.9$. Figure 2(a) presents the amplitude of the E field before it meets the n_e gradient. Once this wave has propagated through the latter [Fig. 2(b)], its wavelength has naturally increased from λ_0 to λ_0/n_r. The amplitude of E also increases from E_0 to $E_0/\sqrt{n_r} \approx 0.89$. This shows that no reflection of the wave has occurred on the larger than λ_0 density gradient. We now consider single mode and multimode cases for the n_e spatial modulation. The single mode modulation of n_r^2 is written as $0.2\cos(2\pi x/\lambda_i)$ with $\lambda_1 = 0.7\lambda_B$, $\lambda_2 = \lambda_B$, and $\lambda_3 = 2.8\lambda_B$. The multimode modulation is the sum of the λ_B mode and 24 additional modes, λ_j, such as $0.7\lambda_B \le \lambda_j \le 2.8\lambda_B$. This multimode case approaches a random inhomogeneity [see n_r^2 in Fig. 2(d)]. The modulations are gradually added on the n_r gradient and are nullified elsewhere. At $n_e/n_c \approx 0.5$, $N_i/\overline{n_e}$ can reach 0.2. Such a high unrealistic value was chosen purposely since a lower and more realistic amplitude of the modulation leads to a larger computational domain, and unreadable Fig. 2. For $\lambda_i = \lambda_1$ and λ_3, the asymptotic solution cannot be distinguished from the result presented in Fig. 2(b) and is not presented here. This means that the wave propagation is unaffected by the chosen modulations. For the $\lambda_2 = \lambda_B$ density ripples, the result is drastically different [Fig. 2(c)]. The amplitude of wave on the left of the density gradient has almost doubled in comparison with the smooth case [Fig. 2(b)]. On the right

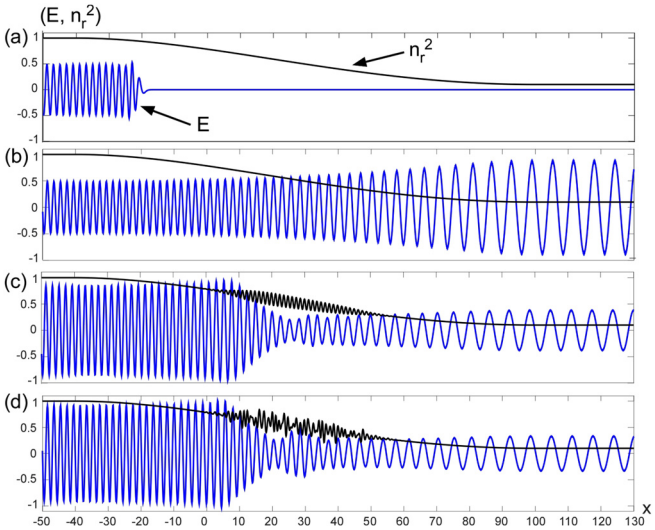

FIG. 2. 1D propagation of an em wave in an inhomogeneous plasma. Wave amplitude (blue curve) as a function of x at t = 280 (a) and t = 648.75 (b)–(d). Square of the plasma index (black curve) for no small-scale modulation (a) and (b), single mode λ_B modulation (c), and multimode modulation including λ_B (d).

of the density gradient, the amplitude of E decreases to 0.39. This means that about 80% of the incoming wave has been reflected by the density ripples. Figure 2(d) presents the result for the multimode modulation. The reflected and transmitted E fields superimpose with the single mode λ_B case. The wave propagation and reflection are unaffected by the added λ_j modulations. As predicted by Eqs. (6) for a multimode n_e inhomogeneity, the em wave self-selects the mode whose wavelength equals to λ_B. Let us underline that the em wave is reflected far from n_c.

V. THE STATIONARY BRAGG REFLECTION

The reflection that has been exhibited here is the Bragg's reflection. Such reflection is the basis of the reflectometry measurements in Tokamak plasma.[32–37] For this diagnostic, a short em pulse is sent into the plasma. This pulse is reflected by moving and very localized plasma fluctuations meeting the Bragg resonance condition [$\lambda(x) = \lambda_B$], and the reflected wave is analyzed. Let us quote a usual comment in the literature about reflectometry: "The scattered signal will *not* originate from the critical density region … the scattering will occur where Bragg resonance condition is satisfied."[32,34,35] As theoretically and numerically demonstrated above, the Bragg reflection can also occur in a stationary plasma for a plane em wave. We will denominate this reflection, the stationary Bragg reflection (SBR). The influence of absorption on the response of the incoming pulse to λ_B fluctuation is usually not considered in reflectometry. However, this question can be tackled by solving Eqs. (5) for $\widetilde{k_i}$. For $\nu_{ei}/\omega_0 \ll 1$, we obtain $\widetilde{k_i} \approx \frac{\overline{\omega_p}^2}{c^2}\frac{x}{2}\frac{N_2}{\overline{n_e}}\cos(2\overline{k_r}\,x)$. Using Eq. (4) for $\overline{k_i}$, $|E|^2$ is written as $|E|^2 = E_0^2\, e^{k_0\, x\frac{\overline{n_e}}{n_c}\left[-\frac{\nu_{ei}/\omega_0}{\sqrt{1-\overline{n_e}/n_c}} + k_0\frac{x N_2}{2\overline{n_e}}\cos(2\overline{k_r}\,x)\right]}$. As the wave energy is proportional to $|E|^2$, the former expression shows that the laser deposition is modulated by the SBR.

The previous derivations are 1D and assume that the density inhomogeneity, the global density gradient, and the laser trajectory are

aligned. In 2D, if we now assume that the laser makes an angle with the direction of the density gradient, and that the inhomogeneity remains stratified perpendicular to the density gradient with $N_2/\overline{n_e} \ll 1$, the analogy with a multi-layer medium indicates that the reflection of the incoming electromagnetic wave will be specular. As $N_2/\overline{n_e}$ increases, the magnitude of the wave harmonics [Eq. (9)] will be no more negligible. We can thus infer the generation of side-scattering lobes in specific directions. For high magnitude of inhomogeneity, Eqs. (3) show that k_r will nonlinearly depends on k_i, and thus, the selection of wave harmonics will depend on the wave absorption. This means that the scattering can be altered if wave absorption is taken into account. We find again the classic result established in reflectometry: the SBR modifies the location of the turning point of the laser beams. We add that the absorption can alter the expected reflection directions.

VI. DISTINCTION BETWEEN THE BRAGG REFLECTION AND BRILLOUIN/RAMAN PARAMETRIC INSTABILITIES

Reflection due to the interaction between the wave and the plasma also occurs due to Brillouin and Raman parametric instabilities. In these cases, a backscattered wave rises from noise level through its amplification by the interplay between the incoming laser wave and a specific acoustic or ionic wave. Thus, SRS and SBS are nonlinear phenomena. The laser wave can be viewed as the modulator that excites oscillators, the plasma waves.[15] On the other hand, for SBR, the scattered wave does not rise from noise. It simply comes from the bulk reflection of the incoming wave on plasma inhomogeneity. This is a linear phenomenon as no response of the plasma is needed. Should the density inhomogeneities arise from purely hydrodynamic phenomena such as turbulence or shock wave transit, the SBR would immediately occur as opposed to Brillouin or Raman parametric instabilities that would require the coupling with acoustic or ionic waves. In the SBR case, the laser wave can be considered as an oscillator which responds to a modulator, the inhomogeneity of the plasma at the Bragg wavelength. As a result, the SBR can be viewed as a most simple parametric instability.

In our modeling, we assume that the plasma is stationary, and that the SBR arises from homogeneities at rest in the plasma reference frame. In reality, the plasma moves and carries its homogeneities with it. This motion will induce a small Doppler frequency shift of the reflected wave generated by the SBR. If the SBR is generated by the bulk turbulence of a gold bubble in an ICF *Hohlraum*, a permanent blue frequency shift should be observed. If the SBR is generated near n_c, and if an ignition-type laser pulse is considered, the frequency shift should go from blue at low laser intensity to red in the main rise of the laser pulse (as the critical surface is pushed back). Given that the plasma velocity in ICF *Hohlraum* remains on the order of 10^7 cm/s, the frequency shift should remain small ($\Delta\lambda \approx 2$Å for $\lambda_0 = 0.35\,\mu$m) in comparison with classic Brillouin frequency shift. A small value of the frequency shift can be experimentally measured[3,38] on laser facilities such as the Laser MegaJoule (LMJ) or the National Ignition Facility (NIF). Such measurements could help determine whether the Bragg reflexion superimposes with the Brillouin instability, and what its magnitude is.

VII. INHOMOGENEITY IN A GOLD PLASMA BUBBLE

The stationary Bragg reflexion needs small-scale density inhomogeneities in the plasma to occur. In this part, we assess the existence of such density variation in the gold bubble which is created by the laser heating of a *Hohlraum*. The "small" scales that we consider are of the order of the local laser wavelength, $\lambda(x)$, which increases with the local electronic density. Thus, these scales can be far greater than λ_0.

In 2019, experiments[39] were performed on the Omega EP[40] laser facility in order to study the expansion of gold plasma due to laser heating. The wavelength of the laser beam is $\lambda_0 = 0.35\,\mu$m. These experiments were designed in a 1D axi-symmetrical geometry. This suppresses any CBET or light bending issues. The beam best focus was targeted on the back surface of the *Hohlraum*. In this paper, only plain gold wall is considered for this surface [Fig. 3(a)]. The pulse shape started with a first picket, followed by a lower part (or trough), and ended by a second picket [Fig. 3(b)]. This pulse mimics the foot of an ignition pulse. The levels of SBS and SRS were very low, below the sensitivity of the detectors. The profile of the laser absorption within the gold bubble was diagnosed by time-resolved side-on x-ray images in the 1–6 keV range. In 2021, experiments on the Omega EP facility using similar platform and pulse shape as described above exhibited inhomogeneous gold bubbles:[41] chaotic structures within the bubble were diagnosed by proton radiography during the second picket. The length scale of the structures was about 100 μm.

In order to understand how the gold bubble can became inhomogeneous, let us remark that it is subject to several hydrodynamic instabilities. First, as the bubble expansion is slowed by the fill-gas, shear flow occurs at the gas–gold interface. This interface becomes Kelvin–Helmholtz (K–H) unstable.[17] Second, as the gold bubble expands, a density gradient is created, and $\partial\rho/\partial x > 0$, where ρ is the plasma density (the laser beam comes from the negative x). The pressure gradient can behave differently. Indeed, during the pickets, numerical simulations[42] show that the pressure, P, develops a local maximum at the location of the maximum laser absorption. In this area, the pressure gradient can become locally negative. As a result, a Rayleigh–Taylor (RT) type instability can grow on the density gradient where $\partial\rho/\partial x \times \partial P/\partial x < 0$.[43] As ablation will be at play, modes whose wavenumber is above the cutoff wavenumber will not be directly created by this instability. However, the nonlinear mode coupling[44,45] can generate high wavenumber modes, i.e., small wavelength structures, and the bulk of the gold bubble can develop a wide spectrum of inhomogeneities. Seeds for these instabilities can come from the laser imprint, the shock waves, self-generated magnetic fields, and the ponderomotive force.

In order to estimate the order of magnitude of the smallest eddies which could exist in the gold bubble, we now estimate the distance on which the plasma viscosity begins to be important. Following Refs. 46

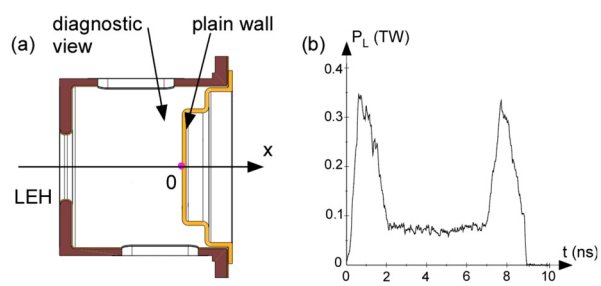

FIG. 3. Details of the 2019 experiments[39] on Omega EP. (a) Sketch of the *Hohlraum*. The laser enters through the laser entrance hole (LEH). (b) Laser pulse.

and 47, this distance reads $l \approx (\nu^3 L/\Delta U^3)^{1/4}$, where ν is the kinematic viscosity, ΔU the fluctuation of the velocity, and L the size of the large eddies. For the 2019 experiments, at t = 8 ns, the mean flow velocity, the dynamic viscosity,[48] and the density in the low density part of the bubble are about $12. \times 10^6$ cm/s, $8. \times 10^{-5}$ Pa s, and 0.0028 g/cm^3, respectively. If a 1% velocity fluctuation and $L \approx 100\,\mu$m are considered, the scale of the smallest eddies is $l \approx 0.19\,\mu$m. We now estimate how long such sub-micron structures can survive to diffusion effect. The lifetime of a structure which is smoothed by diffusion is $\tau_d = l^2/D$, where D is the diffusion coefficient. At t = 8 ns, for the considered plasma, $D = 0.4$ cm^2/s.[48] For $l = \lambda_0/2$, $\tau_d = 0.7$ ns.

Thus, as far as the viscosity is concerned, these structures can be considered as stationary. However, the ionic plasma inhomogeneities will be subjected to the ponderomotive force. The timescale of the ion motion due to this force is of the order of $\tau_{ion} = \omega_{ion}^{-1}$, where $\omega_{ion} = \sqrt{Z\,m_e/(A\,m_p)}\sqrt{n_e/n_c}$ is the ion plasma oscillation frequency, Z the charge number, A the mass number, and m_p the proton mass. Let us define $\tau_{las} = \mathcal{N}\lambda_0/(2\,c)$, the characteristic time required for the laser to interact with $\mathcal{N}$ structures, each of them $\lambda_0/2$ wide. At $n_e/n_c = 0.1$ in a ionized gold bubble in an ICF *Hohlraum*, $\tau_{ion} \approx 50$ fs which is the time the laser needs to interact with $\mathcal{N} \approx 100$ structures. This number increases for lower n_e and less ionized plasma. At higher electronic densities, the ponderomotive force will start to modify the amplitudes N_p of the perturbation spectrum, but without zeroing the N_2 component.

In conclusion, when the Bragg reflexion is considered in an underdense gold plasma, the density inhomogeneity can be considered as quasi-stationary. Furthermore, structures whose size is of the order of the Bragg wavelength can exist and survive long enough to interact with the laser beam.

VIII. POTENTIAL EFFECTS OF THE STATIONARY BRAGG REFLECTION ON ICF PLASMAS

As small-scale inhomogeneity should exist in the gold bubble of the here-above cited experiments, the effect of the stationary Bragg reflection on the laser absorption profile is now studied. In the 2019 experiments, at t = 8 ns, the x-profile of the experimental hard x-ray image disagrees with the numerical one. The experimental emission profile displays a symmetrical increasing/decreasing curve [Fig. 4(a)]. In the 2D rad-hydro numerical simulations,[42] as expected from standard ray-tracing package, the maximum of emission peaks near n_c. Furthermore, the experimental maximum of the laser absorption occurs about 100 μm farther from n_c than predicted by the numerical simulations. In the latter, changes of the electron conduction flux limiter value, the gold equation of state, the Non Local Thermodynamic Equilibrium model, the mesh refinement package, and the number of rays have no significant influence on the emission profile.

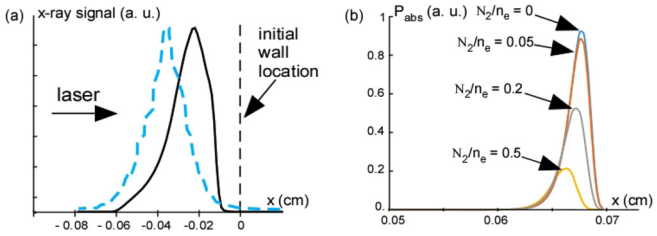

FIG. 4. (a) Experimental and numerical profiles along the symmetry x axis of the side-on x-ray signal in the energy range 1–6 keV at t = 8 ns for a plain wall target[39] in dashed and full lines, respectively. The curves are normalized to their peak values. (b) Absorbed wave power as a function of x for $N_2/n_e = 0,\ 0.05,\ 0.2$, and 0.5.

In order to assess this issue, we model the plasma density as $n_e/n_c(x) = (x/0.0715)^{50}$, $\nu_{ei}/\omega_0(x) = (x/0.075)^{25}$ with x in cm. These simplified profiles are obtained from the numerical results at t = 8 ns. Then, inhomogeneities are added to these profiles. As demonstrated in Secs. II and IV, it is not necessary to consider a full spectrum for the inhomogeneities since the wave self-selects the Bragg mode. So, inhomogeneities are added following only the Bragg resonance condition with $N_2/n_e = 0, 0.05, 0.2$, and 0.5. The high and *a priori* unrealistic values of N_2/n_e are purposely chosen in order to clearly illustrate the SBR effect on the laser absorption. In order to study this effect, the time asymptotic solution of the wave equation is computed. This computation is achieved by modeling the plasma as a succession of homogeneous absorbing layers. Each layer is characterized by its complex index. The E field is written as a superposition of a forward and a backward propagation wave. Using the relations of continuity for E between each layer, the Helmholtz equation for E is solved in each layer. These computation results have been checked against dedicated computations with the Helmholtz package of the Esther code[49,50] which has been validated with analytic test cases.[53] Figure 4(b) presents the resulting averaged power which is locally lost by the wave (the oscillating power has been averaged over a mobile spatial window) for the chosen values of N_2/n_e. For $N_2/n_e = 0$, the power deposition superimposes with the calculation obtained from Eqs. (4) in the framework of the WKB approximation. This means that, for the studied unperturbed profiles, there is no wave reflection, and the laser energy is totally absorbed before reaching the critical surface. As the magnitude of the inhomogeneity increases, more and more power is reflected along the path ($R = 0.04$, 0.37, and 0.73 for $N_2/n_e = 0.05$, 0.2, and 0.5, respectively) and the maximum of the power deposition moves away from n_c. This drift of the deposition location increases with N_2/n_e. As seen in Fig. 4(b), the SBR spontaneously gives a symmetrical deposition profile for high value of N_2/n_e. However, such a high value implies non-negligible backscattered energy.

Since no significant backscattered energy was measured in the 2019 experiments, a sudden occurrence of high-level inhomogeneity seems to be ruled out to explain the discrepancies between experimental and numerical data. Consequently, we prefer to consider a low magnitude inhomogeneity. In this case, a measurable effect on the laser absorption location requires the integration of a small drift over several nanoseconds. The experimental data presented in Fig. 4(a) could be explained by the cumulative SBR effect due to low-level plasma inhomogeneity over several nanoseconds.

The effect of the SBR could lead to other modifications of the plasma properties. Indeed, as the laser deposition is modulated by the Bragg condition (see Sec. V), the subsequent ionization of the plasma will be modulated as such. In areas where the ionization and n_e modulations are in phase, the latter will intensify. This mechanism can lead to an increase in N_2/n_e, and thus reflection. In low to medium absorbing plasma pockets, the superposition of the forward and the backward waves will create beat waves, and transient plasma gratings[54–58] will be generated due to the ponderomotive force. This force could further enhance the amplitude of the density inhomogeneity, leading to a positive feedback (instability) of SBR. The oscillatory speed of the electrons

could become no more negligible with respect to the thermal velocity. The electron heat conduction, and the electron–ion collision frequency will be modified in such plasma pockets.[8,10]

IX. CONCLUSION

In ICF plasmas, micron-scale density inhomogeneity can develop due to hydrodynamic instabilities or turbulence.[18,21] This development can occur within the gold bubble of an *Hohlraum* wall[7,8,17] where the laser is absorbed, and converted to x-rays. In rad-hydro codes, the effects of such inhomogeneity on the laser absorption are not considered. Indeed, even if the mesh was refined enough to describe the λ-scale, the ray-tracing algorithms are based on the WKB approximation, which cannot compute the reflection due to λ-scale variation of the plasma index. Going beyond the WKB approximation, we have theoretically and numerically shown that the laser beam self-selects the Bragg resonance mode in a multimode inhomogeneous ICF plasma. Should the stationary Bragg reflection occur, the location of maximum laser absorption would be moved toward the LEH. This laser drift would then affect the symmetry of the x-ray emission. This reflection differs from classical ICF parametric instabilities. Indeed, the SBR depends on the level of density inhomogeneity which can be solely driven by the hydrodynamics. This means that the strategies currently used to reduce Brillouin and Raman parametric instabilities, such as lowering the laser intensity and the density of the gas-fill, will have no direct effect on the Bragg reflection. We have shown how the energy deposition is modulated by the Bragg reflection. As a consequence, this reflection can create a positive feedback on the density inhomogeneities, leading to instability. This reflection is a good candidate to explain discrepancies between experiments and numerical simulations about the laser trajectory, x-ray emission,[7] energy deposition, and heat transport.

Future works will focus on the 2D SBR with stratified and random density inhomogeneity. New diffraction effects are expected. Sharing experience with the Tokamak communities will be helpful. Indeed, adapting a reflectometry code[59] seems a natural first step. Particle in cell codes are also considered. By revisiting still puzzling experimental data,[7,8] this work will clarify the contribution of the stationary Bragg reflection to laser propagation and deposition in ICF plasmas.

ACKNOWLEDGMENTS

The authors thank J. Griffond for the fruitful discussions on turbulence.

AUTHOR DECLARATIONS

Conflict of Interest

The authors have no conflicts to disclose.

Author Contributions

Marc Vandenboomgaerde: Conceptualization (lead); Supervision (lead); Validation (lead); Writing – original draft (lead); Writing – review & editing (lead). **Cedric Courtois:** Resources (equal). **Josselin Garnier:** Conceptualization (lead); Formal analysis (lead); Resources (equal); Software (equal); Writing – review & editing (equal). **Hui Chen:** Data curation (equal); Resources (equal); Writing – review & editing (equal). **Michel Casanova:** Conceptualization (lead); Software (equal). **Fabrice Chaland:** Conceptualization (supporting); Resources (equal). **Max Bonnefille:** Conceptualization (supporting); Supervision (equal). **Alain Grisollet:** Conceptualization (equal). **Laurent Videau:** Formal analysis (equal); Software (equal); Visualization (equal). **Sylvie Depierreux:** Data curation (equal); Resources (equal). **Veronique Tassin:** Data curation (equal); Resources (equal). **Jean-Pierre Leidinger:** Resources (equal).

DATA AVAILABILITY

The data that support the findings of this study are available within the article.

REFERENCES

[1] S. A. MacLaren, M. B. Schneider, K. Widmann, J. H. Hammer, B. E. Yoxall, J. D. Moody, P. M. Bell, L. R. Benedetti, D. K. Bradley, M. J. Edwards *et al.*, "Novel characterization of capsule x-ray drive at the National Ignition Facility," Phys. Rev. Lett. **112**, 105003 (2014).

[2] L. F. Berzak Hopkins, S. Le Pape, L. Divol, N. B. Meezan, A. J. Mackinnon, D. D. Ho, O. S. Jones, S. Khan, J. L. Milovich, J. S. Ross *et al.*, "Near-vacuum hohlraums for driving fusion implosions with high density carbon ablators," Phys. Plasmas **22**, 056318 (2015).

[3] D. Turnbull, P. Michel, J. E. Ralph, L. Divol, J. S. Ross, L. F. Berzak Hopkins, A. L. Kritcher, D. E. Hinkel, and J. P. Moody, "Multibeam seeded Brillouin side-scatter in inertial confinement fusion experiments," Phys. Rev. Lett. **114**, 125001 (2015).

[4] D. A. Callahan, O. A. Hurricane, J. E. Ralph, C. A. Thomas, K. L. Baker, L. R. Benedetti, L. F. Berzak Hopkins, D. T. Casey, T. Chapman, C. E. Czajka *et al.*, "Exploring the limits of case-to-capsule ratio, pulse length, and picket energy for symmetric hohlraum drive on the National Ignition Facility Laser," Phys. Plasmas **25**, 056305 (2018).

[5] J. E. Ralph, O. Landen, L. Divol, A. Pak, T. Ma, D. A. Callahan, A. L. Kritcher, T. Döppner, D. E. Hinkel, C. Jarrott *et al.*, "The influence of hohlraum dynamics on implosion symmetry in indirect drive inertial confinement fusion experiments," Phys. Plasmas **25**, 082701 (2018).

[6] L. A. Pickworth, T. Döppner, D. E. Hinkel, J. E. Ralph, B. Bachmann, L. P. Masse, L. Divol, L. R. Benedetti, P. M. Celliers, H. Chen *et al.*, "Application of cross-beam energy transfer to control drive symmetry in ICF implosions in low gas fill *Hohlraums* at the National Ignition Facility," Phys. Plasmas **27**, 102702 (2020).

[7] H. Chen, M. Vandenboomgaerde, and O. S. Jones, "Advances in mapping of x-ray emission from NIF hohlraums," High Energy Density Phys. **36**, 100793 (2020).

[8] H. Chen, M. Vandenboomgaerde, and O. S. Jones, "Understanding ICF hohlraums using NIF gated laser-entrance-hole images," Phys. Plasmas **27**, 022702 (2020).

[9] N. Izumi, D. T. Woods, N. B. Meezan, J. D. Moody, O. L. Landen, L. Divol, H. Chen, D. A. Callahan, M. Hohenberger, A. L. Kritcher *et al.*, "Low mode implosion symmetry sensitivity in low gas-fill NIF cylindrical hohlraums," Phys. Plasmas **28**, 022706 (2021).

[10] N. B. Meezan, D. T. Woods, N. Izumi, H. Chen, H. A. Scott, M. B. Schneider, D. A. Liedahl, O. S. Jones, G. B. Zimmerman, J. D. Moody *et al.*, "Evidence of restricted heat transport in National Ignition Facility hohlraums," Phys. Plasmas **27**, 102704 (2020).

[11] W. L. Kruer, S. C. Wilks, B. B. Afeyan, and R. K. Kirkwood, "Energy transfer between crossing laser beams," Phys. Plasmas **3**, 382 (1996).

[12] P. Michel, S. H. Glenzer, L. Divol, D. K. Bradley, D. Callahan, S. Dixit, S. Glenn, D. Hinkel, R. K. Kirkwood, J. L. Kline *et al.*, "Symmetry tuning via controlled crossed-beam energy transfer on the National Ignition Facility," Phys. Plasmas **17**, 056305 (2010).

[13] E. L. Dewald, J. L. Milovich, P. Michel, O. L. Landen, J. L. Kline, S. Glenn, O. Jones, D. H. Kalantar, A. Pak, H. F. Robey *et al.*, "Early-time symmetry in the presence of cross beam energy transfer in ICF experiments on the National Ignition Facility," Phys. Rev. Lett. **111**, 235001 (2013).

[14] D. J. Y. Marion, A. Debayle, P.-E. Masson-Laborde, P. Loiseau, and M. Casanova, "Modeling crossed-beam energy transfer for inertial confinement fusion," Phys. Plasmas **23**, 052705 (2016).

[15] W. L. Kruer, *The Physics of Laser Plasma Interaction* (Addison-Wesley, Redwood City, 1988).

[16]J. F. Drake, P. K. Kaw, Y. C. Lee, G. Schmidt, C. S. Liu, and M. N. Rosenbluth, "Parametric instabilities of electromagnetic waves in plasmas," Phys. Fluids **17**, 778 (1974).
[17]M. Vandenboomgaerde, M. Bonnefille, and P. Gauthier, "The Kelvin-Helmholtz instability in National Ignition Facility hohlraums as a source of gold-gas mixing," Phys. Plasmas **23**, 052704 (2016).
[18]N. Kang, A. Lei, H. Liu, S. Ji, and S. Zhou, "Observation of perturbations in underdense plasmas induced by ablative Rayleigh-Taylor instability," Phys. Plasmas **27**, 112702 (2020).
[19]H. F. Robey, Y. Zhou, A. C. Buckingham, P. Keiter, B. A. Remington, and R. P. Drake, "The time scale for the transition to turbulence in a high Reynolds number, accelerated flow," Phys. Plasmas **10**, 614–622 (2003).
[20]Y. Zhou, "Unification and extension of the similarity scaling criteria and mixing transition for studying astrophysics using high energy density laboratory experiments or numerical simulations," Phys. Plasmas **14**, 082701 (2007).
[21]G. Rigon, B. Albertazzi, T. Pikuz, P. Mabey, V. Bouffetier, N. Ozaki, T. Vinci, F. Barbato, E. Falize, Y. Inubushi *et al.*, "Micron-scale phenomena observed in a turbulent laser-produced plasma," Nat. Commun. **12**, 2679 (2021).
[22]V. L. Ginzburg, *The Propagation of Electromagnetic Waves in Plasmas* (Pergamon Press, 1964).
[23]R. B. White and F. F. Chen, "Amplification and absorption of electromagnetic waves in overdense plasmas," Plasma Phys. **16**, 565–587 (1974).
[24]H. Hora, *Physics of Laser Driven Plasmas* (Wiley-Interscience, 1981).
[25]M. Born and E. Wolf, *Principles of Optics* (Pergamon Press, 1959).
[26]G. Koppelmann, "Zur Theorie der Wechselschichten aus schwachabsorbierenden Substanzen und ihre Verwendung als Interferometerspiegel," Ann. Phys. **460**, 388 (1960) (in German).
[27]C. K. Carnaglia and J. H. Apfel, "Maximum reflectance of multilayer dielectric mirrors in the presence of slight absorption," J. Opt. Soc. Am. **70**(5), 523 (1980).
[28]H. R. Bilger, P. V. Wells, and G. E. Stedman, "Origins of fundamental limits for reflection losses at multilayer dielectric mirrors," Appl. Opt. **33**(31), 7390 (1994).
[29]J. Lekner, "Reflection by absorbing periodically stratified media," J. Opt. **16**, 035104 (2014).
[30]P. Yeh, *Optical Waves in Layered Media*, Wiley Series in Pure and Applied Optics (Wiley, 2005).
[31]D. Euvrard, *Numerical Solution of Partial Differential Equations, Finite Differences, Finite Elements, and Singularity Method*, 2nd ed. (Masson, Paris, 1990) (in French).
[32]N. Bretz, "One-dimensional modeling of the wavelength sensitivity, localization, and correlation in reflectometry measurements of plasma fluctuations," Phys. Fluids B **4**(8), 2414 (1992).
[33]M. E. Manso, "Reflectometry in fusion devices," Plasma Phys. Controlled Fusion **35**, B141 (1993).
[34]J. H. Irby, S. Home, I. H. Hutchinson, and P. C. Stek, "2D full-wave simulation of ordinary mode reflectometry," Plasma Phys. Controlled Fusion **35**, 601 (1993).
[35]B. B. Afeyan, A. E. Chou, and B. I. Cohen, "The scattering phase shift due to Bragg resonance in one-dimensional fluctuation reflectometry," Plasma Phys. Controlled Fusion **37**, 315 (1995).
[36]C. Fanack, I. Boucher, F. Clairet, S. Heuraux, G. Leclert, and X. L. Zou, "Ordinary-mode reflectometry: Modification of the scattering and cut-off responses due to the shape of localized density fluctuations," Plasma Phys. Control Fusion **38**, 1915 (1996).
[37]T. L. Rhodes, W. A. Peebles, E. J. Doyle, P. Pribyl, M. Gilmore, R. A. Moyer, and R. D. Lehmer, "Signal amplitude effects on reflectometer studies of density turbulence in tokamaks," Plasma Phys. Controlled Fusion **40**, 493 (1998).
[38]S. Depierreux, D. T. Michel, V. Tassin, P. Loiseau, C. Stenz, and C. Labaune, "Effect of the laser wavelength on the saturated level of the stimulated Brillouin scattering," Phys. Rev. Lett. **103**, 115001 (2009).
[39]S. Depierreux, V. Tassin, D. Antigny, R. E. Bahr, N. Botrel, R. Bourdenet, G. DeDemo, L. DeLaval, O. Dubos, J. Fariaut *et al.*, "Experimental evidence of harnessed expansion of a high-Z plasma using the hollow wall design for indirect drive inertial confinement fusion," Phys. Rev. Lett. **125**, 255002 (2020).
[40]J. H. Kelly, L. J. Waxer, V. Bagnoud, I. A. Begishev, J. Bromage, B. E. Kruschwitz, T. J. Kessler, S. J. Loucks, D. N. Maywar, R. L. McCrory *et al.*, "OMEGA EP: High-energy petawatt capability for the OMEGA laser facility," J. Phys. IV **133**, 75 (2006).
[41]J. P. Leidinger and C. Courtois, private communication (2023).
[42]E. Lefebvre, S. Bernard, C. Esnault, P. Gauthier, A. Grisollet, P. Hoch, L. Jacquet, G. Kluth, S. Laffite, S. Liberatore *et al.*, "Development and validation of the TROLL radiation-hydrodynamics code for 3D hohlraum calculations," Nucl. Fusion **59**, 032010 (2019).
[43]S. Chandrasekhar, *Hydrodynamic and Hydromagnetic Stability* (The Clarendon Press, Oxford, 1968).
[44]S. W. Haan, "Weakly nonlinear hydrodynamic instabilities in inertial fusion," Phys. Fluids B **3**(8), 2349–2355 (1991).
[45]J. Garnier, P.-A. Raviart, C. Cherfils-Clérouin, and L. Masse, "Weakly nonlinear theory for the ablative Rayleigh-Taylor instability," Phys. Rev. Lett. **90**, 185003 (2003).
[46]L. D. Landau and E. M. Lifshitz, *Fluids Mechanics* (Pergamon Press, 1959).
[47]A. N. Kolmogorov, "The local structure of turbulence in incompressible viscous fluid for very large Reynolds numbers," Proc. Math. Phys. Sci. **434**, 9–13 (1991).
[48]P. Arnault, "Modeling viscosity and diffusion of plasma for pure elements and multicomponent mixtures from weakly to strongly coupled regimes," High Energy Density Phys. **9**, 711–721 (2013).
[49]S. Bardy, B. Aubert, T. Bergara, L. Berthe, P. Combis, D. Hébert, E. Lescoute, Y. Rouchausse, and L. Videau, "Development of a numerical code for laser-induced shockwaves applications," Opt. Laser Technol. **124**, 105983 (2020).
[50]L. Videau, "Study of laser-matter interaction from solid to plasma," Report No. FRCEA-TH-14764, 2020 (in French).
[51]H. Hora, "Optical constants of fully ionized hydrogen plasma for laser radiation," Nucl. Fusion **10**, 111 (1970).
[52]P. Mora, "Theoretical model of absorption of laser light by a plasma," Phys. Fluids **25**(6), 1051 (1982).
[53]L. M. Brekhovskikh and R. T. Bayer, *Waves in Layered Media*, Applied Mathematics and Mechanics Vol. 16, 2nd ed. (Academic Press, 1980).
[54]Z.-M. Sheng, J. Zhang, and D. Umstadter, "Plasma density gratings induced by intersecting laser pulses in underdense plasmas," Appl. Phys. B. **77**, 673 (2003).
[55]S. Monchocé, S. Kahaly, A. Leblanc, L. Videau, P. Combis, F. Réau, D. Garzella, P. D'Oliveira, P. Martin, and F. Quéré, "Optically controlled solid-density transient plasma gratings," Phys. Rev. Lett. **112**, 145008 (2014).
[56]G. Lehmann and K. H. Spatschek, "Transient plasma photonic crystals for high-power lasers," Phys. Rev. Lett. **116**, 225002 (2016).
[57]J. R. Smith, C. Orban, G. K. Ngirmang, J. T. Morrison, K. M. George, E. A. Chowdhury, and W. M. Roquemore, "Particle-in-cell simulations of density peak formation and ion heating from short pulse laser-driven ponderomotive steepening," Phys. Plasmas **26**, 123103 (2019).
[58]C. Zhang, Z. Nie, Y. Wu, M. Sinclair, C.-K. Huang, K. A. Marsh, and C. Joshi, "Ionization induced plasma gratings and its applications in strong-field ionization measurements," Plasma Phys. Controlled Fusion **63**, 095011 (2021).
[59]S. Heuraux, E. Faudot, F. da Silva, J. Jacquot, L. Colas, S. Hacquin, N. Teplova, K. Syseova, and E. Gusakov, "Study of wave propagation in various kinds of plasmas using adapted simulation methods, with illustrations on possible future applications," C. R. Phys. **15**, 421 (2014).